Soil Biochar Quantification via Hyperspectral Unmixing

Citation for published version:
Tong, Lei, Zhou, Jun, Xu, C Y, Qian, Yuntao, Gao, Yongsheng (2013) Soil Biochar Quantification via Hyperspectral Unmixing. Proceedings of the 2013 Digital Image Computing Techniques and Applications International Conference, Hobart, Australia, 26-28 November 2013, pp.1-8.

Soil Biochar Quantification via Hyperspectral Unmixing

Lei Tong[1] Jun Zhou[2] Chengyuan Xu[3] Yuntao Qian[4] Yongsheng Gao[1]

[1]School of Engineering, Griffith University, Nathan, QLD 4111, Australia
[2]School of ICT, Griffith University, Nathan, QLD 4111, Australia
[3]Environmental Futures Centre, Griffith University, Nathan, QLD 4111, Australia
[4]College of Computer Science, Zhejiang University, Hangzhou, 310027, P. R. China

Abstract

Biochar has unique function to improve soil chemo-physical and biological properties for crop growth. Because changes of biochar in soil may affect its long-term effectiveness as an amendment, it is important to quantify and monitor biochar after application. In this paper, we propose a solution for this problem via hyperspectral image analysis. We treat the soil image as a mixture of soil and biochar signals, and then apply hyperspectral unmixing methods to predict the biochar abundance at each pixel. The final percentage of biochar can be calculated by taking the mean of the abundance of hyperspectral pixels. We have compared several hyperspectral unmixing methods based on least squares estimation and nonnegative matrix factorization with various sparsity constraints. Experimental results are evaluated by polynomial regression and root mean square errors against the ground truth data collected in the environmental labs. The results show that hyperspectral unmixing is a promising method to measure the percentage of biochar in the soil.

1 Introduction

Food security is a key global concern for the 21st century. With growing world population and rising living standard, global demand for agricultural products will rise 70% by 2050 [1], while agricultural productivity is facing emerging plateau and high exposure to climate change [9]. Thus, there is an imperative need for farming approaches that can efficiently use constrained resources (e.g. land and water) and effectively mitigate greenhouse gas emissions. Soil amendment with biochar, a carbon-rich product of burning biomass in the absence of air, is recognised globally as an emerging approach to improve soil fertility [20]. As an effective soil amendment, biochar has unique functions to improve soil chemo-physical and biological properties for crop growth [3]. These positive effects of biochar on crop yield are especially significant in degraded soils [17]. Biochar also has high proportion of recalcitrant C with hundreds to thousands of years of durability, making it a potentially effective soil C sink [4, 11]. Agronomic benefits of biochar and the potential of biochar for soil carbon sequestration have been widely demonstrated in many on-ground trials over the world [17, 2].

However, biochar has heterogeneous and complex chemical composition and a high proportion of carbon is non-reactive. These properties make it analytically challenging to accurately quantify biochar within soil. Currently, biochar in soils is normally measured by determination of (1) extractable compounds which are characteristic for biochar, (2) residual stable carbon after oxidizing reactive carbon with chemical or thermal approaches, and (3) thermal decomposition behaviour of different carbon fractions in soil [12]. Most of these analytical approaches are laborious, time-consuming and heavily-dependent on specific equipments; some can be expensive. For routine quantification of biochar in soils, more rapid and economic methods need to be developed. Recently, spectroscopic methods have been developed to quantify various carbon fractions (e.g. total organic carbon) in soil [8, 5]. These approaches are sufficiently rapid to analyse large amount of soil samples at a reasonable cost. Nonetheless, up-to-date, no spectroscopic approach has been tested specifically for quantifying biochar that is artificially applied to soil.

In this paper, we explore hyperspectral image analysis method for biochar quantification in soil. Hyperspectral images have been used in remote sensing for many years. They have shown great advantages in land analysis, mining, and field surveillance due to the rich spectral information in the images. Hyperspectral unmixing is the technique of analysing the proportion of constituents or endmembers in images. This technique can be naturally applied in estimating the percentage of the biochar in soil because soil images can be considered as mixtures of both soil and biochar endmembers.

Many hyperspectral unmixing methods have been pro-

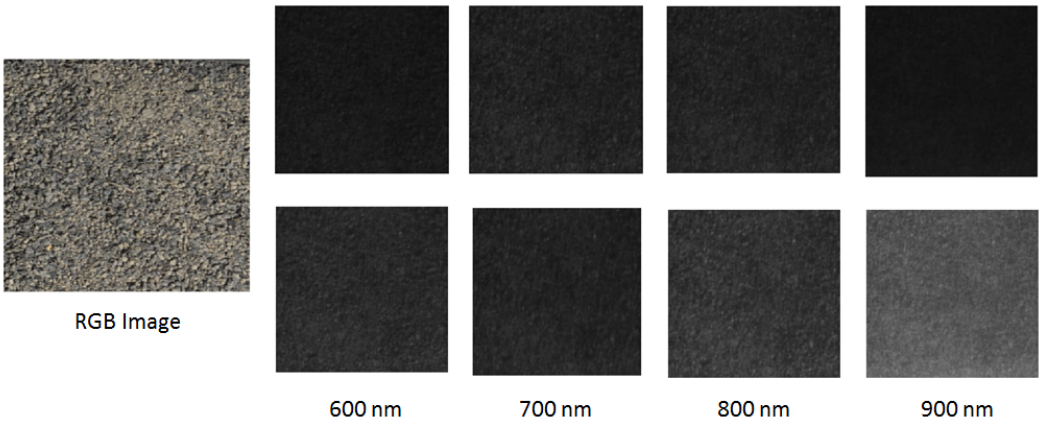

Figure 1. Image samples of soil mixed with biochar. On the left-hand side is an RGB image. On the right-hand side are the uncalibrated and calibrated sample band images.

posed during the past years. N-FINDR [19], as one of the earliest unmixing methods, finds the biggest simplex to estimate the endmembers and their abundances. Vertex component analysis [13] analyses the vertices in the simplex in order to find the optimal endmembers. Independent component analysis [18] uses mutual information to measure the statistical independency of endmembers. More recently, nonnegative matrix factorization (NMF) [14] has attracted much attention. It treats the unmixing as a blind source separation problem, and estimates both endmembers and abundances simultaneously.

In the problem targeted by this paper, the unmixing problem reduces to abundance estimation because we can acquire the pure soil and biochar spectrum. This implies that we can explore least squares method to estimate the abundances directly [6]. However, we also need to consider several important mixing properties. Firstly, the percentages of both soil and biochar shall not be negative. This is natural because the lowest proportion of an endmember in a pixel shall be larger than or equal to zero. Secondly, the sum of the abundances at each pixel shall be added to unity. Thirdly, it is expected that the abundance matrix shall be sparse so that most pixels tend to have only a pure endmember. These three properties are consistent with the constraints normally imposed on NMF solutions [15]. Therefore, we build our method based on the constrained NMF method but fix the endmembers using pure soil and biochar spectral signatures. Several models with and without sparsity constraints are implemented and compared. The results show that these models are effective while $L_{1/2}$ sparsity constraint has generated the best performance. This method is much easier to be conducted than other methods such as thermal decomposition and mid-infrared spectroscopy [8, 5] which have been applied to soil carbon analysis but are normally performed on only a few pixel samples other than the whole image.

The rest of this paper is organised as follows. In Section 2, a brief overview of the proposed method is given. Section 3 introduces the unmixing methods. Section 4 presents the experimental results. Finally, the conclusions are drawn in Section 5.

2 Method Overview

The proposed method of detecting biochar within soil consists of three steps: (1) image pre-processing; (2) hyperspectral unmixing; and (3) polynomial regression.

The main goal of the pre-processing step is to calibrate the hyperspectral image so that it is not influenced by the variations of illumination condition. In this step, a calibration board which reflects 99% of the light is used to provide information on the light source. Each band image is normalised against the corresponding band image of the calibration board in order to get consistent spectral measurement. Figure 1 shows an example of such calibration step. On the left-hand side is a color image captured by a traditional RGB camera. In all other columns, the first row shows some band images before calibration, while the second row shows the calibrated images. Figure 2 displays the mean spectrum of pixels in soil images with different proportion of biochar. Clear tendency can be observed on the changes of spectrum responses with respect to biochar quantity in the soil.

In the hyperspectral unmixing step, a fully constrained least squares based linear unmixing model is firstly introduced [7]. This method miminises the pixel-wise differ-

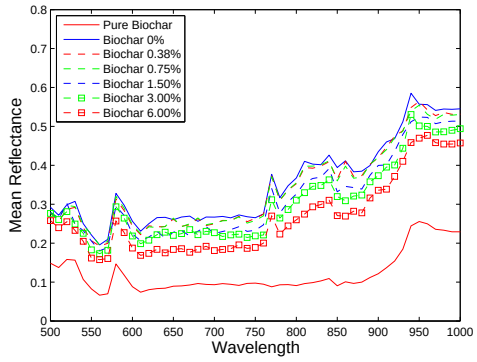

Figure 2. Mean spectrum of dry soil samples with different percentage of biochar.

ences between the observed image and the estimated mixed pixels, while maintaining the full additivity condition. Then we propose a modified sparsity constrained NMF method based on [15]. In this model, we used pure soil and biochar spectral signatures as the endmembers, and estimates their abundances using an iterative optimisation step which updates the abundance matrix recursively until termination conditions have been met. Then the mean of the pixel-wise abundances is calculated to generate the whole image biochar estimation. To compare the effectiveness of different sparsity constraints, we have applied both L_1 and $L_{1/2}$ norm to control the sparsity of the abundance matrix.

The estimation generated from the unmixing step is the volume of the biochar. We have to convert it to percentage in terms of weight. To do so, in the final step, we used a polynomial regression approach to convert the biochar volume to weight fraction.

3 Unmixing Methods

In this section, we first define a linear spectral mixture model, then provide detailed introduction on the three unmixing methods mentioned in Section 2. We also present the polynomial regression method for volume to weight conversion.

3.1 Linear Spectral Mixture Model

Each pixel in a hyperspectral image can be considered as the mixture of several endmembers. Let the number of wavelength-indexed bands in an image be H and the number of endmembers be K. A pixel y in a hyperspectral image is an $H \times 1$ column vector whose entries correspond to the reflectance of objects in different bands. Let M be an $H \times K$ matrix $(m_1, \ldots, m_j, \ldots, m_K)$, where m_j is an $H \times 1$ column vector representing the spectral signature of the j^{th} endmember. Then y can be approximated by a linear combination of endmembers

$$y = Mr + e \tag{1}$$

where r is a $K \times 1$ column vector for endmember abundances, and e is the additive Gaussian white noise.

It is natural to extend the above pixel-level mixing model to the whole image. Let N be the number of pixels contained in a hyperspectral image Y, the linear model becomes

$$Y = MR + E \tag{2}$$

where matrices Y, R, and E represent the hyperspectral image, the abundance matrix, and the additive noise, respectively.

The goal of general hyperspectral unmixing method is estimating both M and R from Y. In the biochar quantification problem addressed in this paper, because the endmember signatures can be calculated from pure soil and biochar images, both Y and M are known in advance. Therefore, our goal is to estimate the abundance matrix R only.

3.2 Least Squares Linear Unmixing

Least squares is a common solution for regression analysis. The goal is to minimise the differences between observed and estimated image data $\|y - Mr\|^2$. Assuming there is no additive white Gaussian noise, unconstrained least squares for unmixing is defined as

$$\hat{r}^U = (M^T M)^{-1} M^T y. \tag{3}$$

The drawback of unconstrained least squares method is that M should be full column rank and that it does not meet full additivity condition, i.e., all endmember abundances sum to one at each pixel. To solve these problems, general least squares methods were proposed with full additivity constraint have been proposed [6, 10], which can be expressed as

$$Q = (y - Mr)(y - Mr)^T - \lambda(\sum_{i=1}^{k} r(i) - 1) \tag{4}$$

where λ is an intermediate parameter used in computation. By minimising Q with respect to r, we get

$$\hat{r}^F = \hat{r}^U - (M^T M)^{-1} S^T [S(M^T M)^{-1} S^T]^{-1} (S\hat{r}^U - b) \tag{5}$$

where $b = 1$, S is a $1 \times K$ row vector whose entries are all ones.

The fully constrained least squares is an iterative method. It first calculates $\hat{r}^U$ using equation (3), which is then used to calculate $\hat{r}^F$ from equation (5). If all components in $\hat{r}^F$

are positive, the iteration stops. Otherwise, each negative $\hat{r}^F$ is divided by its corresponding component in vector $s = (M^T M)^{-1} S$ and $|\hat{r}_j^F / s_j|$ that has the largest absolute value is determined. The next step is setting $\hat{r}_j = 0$ and removing its corresponding endmember signature m_j from M. The method then goes back to the first step and reiterates the whole process.

3.3 Sparsity Constrained Nonnegative Matrix Factorization with Known Endmembers

As mentioned in Section 2, NMF method is also chosen to perform hyperspectral unmixing. Using the linear mixture model, NMF can minimise the difference between Y and MR and force the M and R to be nonnegative. The Euclidean distance is used here to measure such difference. The object function of NMF based on Euclidean distance is defined as follows [14]:

$$obj(M, R) = \frac{1}{2}\|Y - MR\|_2^2 \tag{6}$$

It has been proved that this object function can not generate a unique globally optimal solution for both M and R [15]. Therefore, NMF is always used with constraints such as additivity and sparsity. The object function with sparsity constraint is

$$obj(M, R) = \frac{1}{2}\|Y - MR\|_2^2 + \lambda\|R\|_p \tag{7}$$

where $\lambda \in R^+$ is a scalar that controls the sparsity of abundance matrix R, and p indicates a $p-$norm of the abundance matrix.

After the object function has been obtained, the optimal solution can be computed using algorithms such as gradient decent or others. Here, we follow the optimisation scheme proposed in [15] which iteratively updates M and R while fixing the other parameter unchanged. This scheme is based on the multiplicate update rule for standard NMF and it is proved to be converging [16]. For Equation (6) the multiplicative update becomes

$$M \leftarrow M. * YR^T./MRR^T \tag{8}$$

$$R \leftarrow R. * M^T Y./M^T MR \tag{9}$$

where$(.)^T$ is the transpose of the matrix, $.*$ and $./$ denote element-wise multiplication and division, respectively.

When L_p sparsity constraint is applied, the optimisation solution is as follows

$$M \leftarrow M. * YR^T./MRR^T \tag{10}$$

$$R \leftarrow R. * M^T Y./(M^T MR + \frac{\lambda}{2}R^{p-1}) \tag{11}$$

To meet the fully additivity constraint, the method in [7] is employed where the data matrix Y and the signature matrix M are replaced by Y_f and M_f which are augmented matrices by a row of constants defined as follows

$$Y_f = \begin{pmatrix} Y \\ \delta 1_N^T \end{pmatrix} \tag{12}$$

$$M_f = \begin{pmatrix} M \\ \delta 1_N^T \end{pmatrix} \tag{13}$$

where δ is a parameter to balance the impact of the additivity constraint on the abundance matrix. A large δ forces the sum of abundances at each pixel closer to unity.

In the application of soil biochar quantification, as the endmember of soil and biochar can ge obtained by taking images of pure soil and biochar, we only iterate equation (11). Meanwhile M and M_f are fixed using the pure endmembers.

In this method, we have adopted both L_1 and $L_{1/2}$ sparsity constraints. When L_1 constraint is applied, equation (11) becomes

$$R \leftarrow R. * M^T Y./(M^T MR + \lambda) \tag{14}$$

If $L_{1/2}$ sparsity is used, equation (11) becomes

$$R \leftarrow R. * M^T Y./(M^T MR + \frac{\lambda}{2}R^{-\frac{1}{2}}) \tag{15}$$

The procedure of the sparsity constrained unmixing is described below

1. Input M as the endmembers.
2. Randomly initialise R by values between 0 and 1. Rescale each column of R to unit norm.
3. Augment Y and M to Y_f and M_f.
4. Let $obj_{old} = obj(Y_f, R)$.
5. Update R by applying Equation (11), (14) or (15).
6. Let $obj_{new} = obj(Y_f, R)$.

This iteration process continues until the maximum number of iterations is reached or the following condition has been met

$$|obj_{new} - obj_{old}\|_2^2 < \epsilon \tag{16}$$

where $\epsilon = 0.0001$.

Table 1. Correspondence between the percentage of weight and volume of biochar in the soil.

	Biochar Percentage					
Weight	0.00	0.38	0.75	1.50	3.00	6.00
Volume	0.00	3.57	6.93	13.04	23.35	38.60

3.4 Polynomial Regression

After the abundance is estimated, the mean of the abundance of each endmember is calculated, which stands for the volume of the biochar or soil. However, in environmental practice, the weight of the biochar is widely used. The weight to volume conversion can be obtained using polynomial regression method. In this work, we adopted a quadratic polynomial regression model

$$w = a_0 + a_1 v + a_2 v^2 + e \tag{17}$$

where w and v are the weight and volume, respectively. e is an additive noise. This model can be solved by standard least squares estimation

$$\hat{a} = (V^T V)^{-1} V^T W \tag{18}$$

where W is a vector and V is a matrix, both constructed from data samples.

In order to calculate the regression coefficients, we have collected the ground truth percentage of weight and volume of biochar in the soil using devices in the environmental lab. Table 1 shows such ground truth data. After the regression coefficients are obtained, the volume-weight conversion can be easily performed.

4 Experiments

In this section, we introduce the image data used for experiments, and then present the biochar estimation results using the three models described in Section 3.

4.1 Data Collection

The soil used in this experiment is a redoxi-hydrosol with poor agronomic properties, sandy and low in all nutrients. Amendment with biochar is believed to be the most effective in such unproductive soil. The soil was collected near Bundaberg, Queensland, Australia in December 2012 and the paddy was used for sugarcane cropping during the last four years. Before conducting this experiment, the soil was used in a pot trial to examine the effect of soil amendment with biochar on the growth of peanut. Peanuts were grown for five months in this soil mixed with 0%, 0.38%, 0.75%, 1.50%, 3.00 and 6.00 of biochar in weight, whose corresponding volume has been give in Table 1. Then plants were harvested and about 300g of soil was sampled from each pot. The soil was processed with 2mm sieve to get rid of most fine roots and then air dried in an oven at 35°C.

The biochar used in this experiment was produced from peanut shell (Tropic Earth Ltd., Tolga, Queensland, Australia). Raw peanut shell of 8 moisture (provided by Peanut Company of Australia (PCA) Ltd.) was introduced into a proprietary continuous rotary design biochar kiln. The residence time of the feedstock was 5.5 minutes at 550°C $\pm$ 50°C. The biochar is quenched by manual water spray upon exiting the reactor into a 1m steel bin and left to cool overnight.

To capture the hyperspectral soil image, a hyperspectral camera with an acousto-optical tunable filter (AOTF) camera was used. This camera can take hyperspectral images from 400nm to 1000nm wavelength at every 10nm. However, because the signal to noise ratio of wavelength from 400nm to 500nm is too low, these bands were removed in the experiments. Therefore, each hyperspectral image contains 50 bands. Sample soil images and mean spectrum of soils with different percentage of biochar have been given in Figures 1 and 2, respectively.

During the imaging process, to guarantee consistent lighting condition and sufficient illumination intensity, all hyperspectral soil images were taken outdoor in sunny days between 11:00am and 1:00pm. In order to reduce the random effect on uneven mixing of soil and biochar, three hyperspectral images were taken for each soil sample with soil container well shaken before the each image was taken. In total, 18 soil images were collected. A calibration step, which has been introduced in Section 2, was applied to normalise the images before they were used in the unmixing analysis.

4.2 Results

We have implemented all three unmixing methods introduced in Section 3, i.e., fully constrained least squares (Least Squares), L_1 sparsity constrained NMF (L_1 NMF), and $L_{1/2}$ sparsity constrained NMF ($L_{1/2}$ NMF). For both NMF methods, we have set the constraint parameter λ to 0.5. These methods were applied to each hyperspectral image and generated the results shown in Table 2.

In this table, the first column shows the percentage of biochar and soil in terms of weight. Images 1 to 3 are the three images captured for each soil sample. Each column under the image index shows the percentage of either biochar or soil in terms of volume. The last two columns are the mean and standard deviation of the volume estimation on three images. The results show that although three

Table 2. Unmixing results

	Least Squares							
Times	Image 1		Image 2		Image 3		Mean	
Biochar(W%)	Biochar(V%)	Soil(V%)	Biochar(V%)	Soil(V%)	Biochar(V%)	Soil(V%)	Biochar(V%)	Soil(V%)
6.000	41.28	58.72	47.94	52.06	40.50	59.50	43.24±4.09	56.76±4.09
3.000	41.09	58.91	31.65	68.35	36.45	63.55	36.40±4.72	63.60±4.72
1.500	25.04	74.96	24.18	75.82	27.59	72.41	25.60±1.77	74.40±1.77
0.750	9.82	90.18	7.10	92.90	8.02	91.98	8.31±1.38	91.69±1.38
0.375	3.00	97.00	7.02	92.98	3.90	96.10	4.64±2.11	95.36±2.11
	L_1 NMF							
Times	Image 1		Image 2		Image 3		Mean	
Biochar(W%)	Biochar(V%)	Soil(V%)	Biochar(V%)	Soil(V%)	Biochar(V%)	Soil(V%)	Biochar(V%)	Soil(V%)
6.000	40.43	59.17	46.68	52.82	39.39	60.14	42.17±3.94	57.38±3.98
3.000	40.14	59.43	31.12	68.45	35.76	63.78	35.67±4.51	63.89±4.51
1.500	24.67	74.97	23.57	75.97	26.98	72.56	25.07±1.74	74.50±1.75
0.750	10.23	89.49	7.43	92.29	8.42	91.36	8.70±1.42	91.05±1.43
0.375	3.61	96.21	7.40	92.24	4.51	95.30	5.17±1.98	94.58±2.08
	$L_{1/2}$ NMF							
Times	Image 1		Image 2		Image 3		Mean	
Biochar(W%)	Biochar(V%)	Soil(V%)	Biochar(V%)	Soil(V%)	Biochar(V%)	Soil(V%)	Biochar(V%)	Soil(V%)
6.000	34.95	64.64	44.30	55.24	30.53	68.94	36.59±7.03	62.94±7.01
3.000	33.76	65.78	28.02	71.61	33.05	66.56	31.61±3.13	67.98±3.17
1.500	15.57	84.03	12.10	87.33	17.27	82.22	14.98±2.63	84.52±2.59
0.750	4.42	95.36	5.12	94.74	7.08	92.87	5.54±1.38	94.32±1.3
0.375	2.58	97.41	3.23	96.52	3.24	96.75	3.01±0.38	96.89±0.47

images were collected from the same soil sample, due to randomness in the mixing, different percentages of biochar have been generated. On one hand, this suggests that the hyperspectral imaging method is effective in detecting the fine differences between soil images. On the other hand, it implies that in practice, when our hyperspectral imaging method is applied to biochar quantification problem, multiple images of the same soil sample are required to reduce the influence of uneven mixture of soil and biochar.

Table 2 also shows that there is consistent tendency on the percentage of biochar estimated from the images when the weight percentage changes from 0% to 6.00%. This is clearly demonstrated by the mean of the results on three images for each mixing setting. Therefore, all three hyperspectral unmixing methods under comparison have the capability in judging which soil contains more biochar than the others. This verifies the effectiveness of the hyperspectral unmixing methods for biochar quantification. However, these three unmixing methods do show differences in the estimation results. Due to the sparsity constraints, the L_1 NMF has generated lower percentage of biochar and higher percentage of soil than the Least Square method. The $L_{1/2}$ NMF further enforces the sparsity of the solution than the L_1 counterpart.

Figure 3 provides an intuitive illustration on the estimated abundance matrix of several soil samples when Least Squares method is used. In this figure, each panel shows the abundance maps of biochar (left) and soil (right) at each location in the image. The brighter a pixel is, the higher proportion of the corresponding endmember is at the pixel. It can be clearly observed that the brightness of the abundance map of the biochar becomes higher along with the increase of the percentage of biochar in the soil. We also plot the abundance maps in Figure 4 when $L_{1/2}$ NMF is used for estimation. It is not surprising to see that $L_{1/2}$ NMF generates darker biochar abundance map and brighter soil abundance map than the Least Squares estimation.

We performed two experiments for quantitative evaluation of the three hyperspectral unmixing methods introduced in this paper. In the first experiment, we generated regression curves using the polynomial regression method introduced in Section 3. For each unmixing model, we used the estimated biochar volume for each soil sample and the ground truth weight percentage as the input to equation (17). Figure 5 shows the regression results. The red curve represents the ground truth, while the dash blue curve, blue curve, and green curve are the results of the $L_{1/2}$ NMF, the L_1 NMF, and the Least Squares methods, respectively. From this figure, it can be seen that the performance of the L_1 NMF is very close to that of the Least Squares method, which suggests that L_1 sparsity can not further increase the sparsity of the solution in NMF unmixing. This result is consistent with the analysis in [15] that L_1 regularizer is a relaxation of the full additivity constraint. Because this constraint has been incorporated in both L_1 NMF and least squares model, the effect of L_1 regularizer becomes not prominent. $L_{1/2}$ NMF, on the contrary, has demonstrated very close performance to the regression result from the ground truth data, and is significantly better than the other two methods. This suggests that $L_{1/2}$ NMF is a preferred

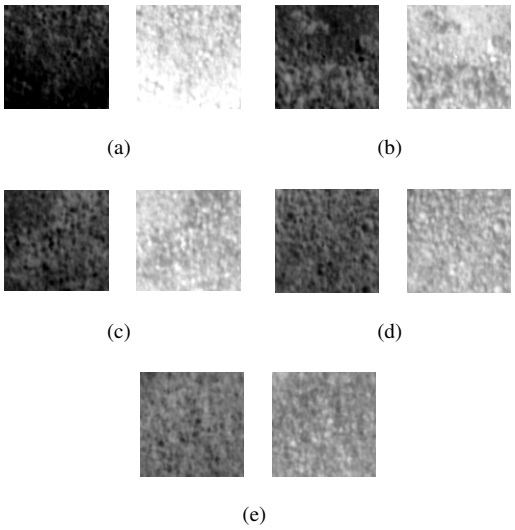

Figure 3. Abundances of different soil samples in terms of volumes of biochar and soil from the Least Squares method. (a) Biochar 0.38%; (b) Biochar 0.75%; (c) Biochar 1.50%;(d) Biochar 3.00%; (e) Biochar 6.00%.

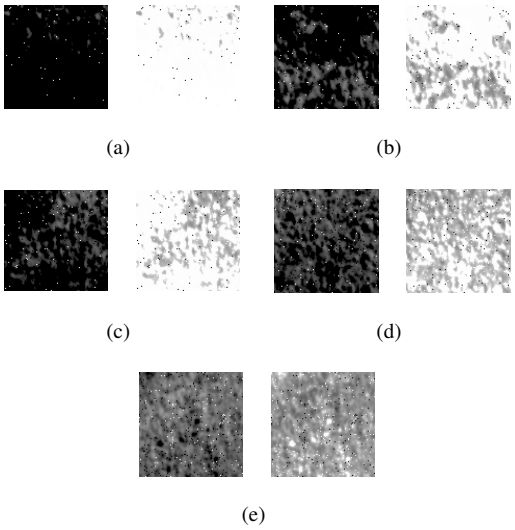

Figure 4. Abundances of different soil samples in terms of volumes of biochar and soil from the $L_{1/2}$ NMF method. (a) Biochar 0.38%; (b) Biochar 0.75%; (c) Biochar 1.50%;(d) Biochar 3.00%; (e) Biochar 6.00%.

solution for the biochar quantification problem.

In the second experiment, we evaluated these three methods using Root Mean Square Errors (RMSE) on the converted weight percentage of biochar. To do so, we generated the regression coefficients using ground truth data, and then applied this regression model to the volume data estimated by the three methods being compared. This is close to the scenario on how hyperspectral imaging based biochar quantification will be deployed in both lab and field environment, i.e., estimating the weight percentage of biochar directly from images. The RMSE from the Least Squares, the L_1 NMF, and the $L_{1/2}$ NMF methods are 1.36, 1.27, and 0.67, respectively. Such results further prove that $L_{1/2}$ NMF is a better option for soil biochar estimation. Regarding the efficiency of these methods, the time costs of the Least Squares, the L_1 NMF, and the $L_{1/2}$ NMF methods are 3.17 seconds, 151.74 seconds, and 68.61 seconds, respectively, when ran on a desktop computer with an Intel Core Duo 2 3.0GHz CPU. The NMF based methods took longer time than the Least Squares counterpart because of the iterative optimization steps.

5 Conclusion

In this paper, we have developed a solution for soil biochar quantification using hyperspectral imagery. This method treats soil images as mixture of soil and biochar, and then uses hyperspectral unmixing models to analyze the percentage of biochar in the soil. The proposed method also enables conversion of biochar volume proportion to weight proportion via a polynomial regression model. We have compared three linear hyperspectral unmixing models and shown that the $L_{1/2}$ sparsity constrained nonnegative matrix factorization method is a better solution than its L_1 counterpart and the fully constrained least squares estimation method. Our results suggest that hyperspectral analysis has strong potential to be developed into a promising approach for rapid quantification of soil biochar.

References

[1] Report of the FAO expert meeting on how to feed the world in 2050. Technical report, Food and Agriculture Organization of the United Nations, Rome, 2009.

[2] C. J. Atkinson, J. D. Fitzgerald, and N. A. Hipps. Potential mechanisms for achieving agricultural benefits from biochar application to temperate soils: a review. *Plant and Soil*, 337(1-2):1–18, 2010.

[3] K. Y. Chan and Z. Xu. Biochar: nutrient properties and their enhancement. *Biochar for environmental management: science and technology. Earthscan, London*, pages 67–84, 2009.

[4] C.-H. Cheng, J. Lehmann, J. E. Thies, and S. D. Burton. Stability of black carbon in soils across a climatic gradient. *Journal of Geophysical Research*, 113(G2):G02027, 2008.

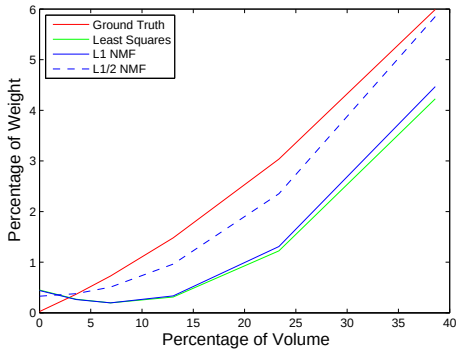

Figure 5. Performance Curve

[5] C. Gomez, R. A. Viscarra Rossel, and A. B. McBratney. Soil organic carbon prediction by hyperspectral remote sensing and field VIS-NIR spectroscopy: An Australian case study. *Geoderma*, 146(3):403–411, 2008.

[6] D. Heinz, C.-I. Chang, and M. Althouse. Fully constrained least-squares based linear unmixing [hyperspectral image classification]. In *Proceedings of the IEEE International Geoscience and Remote Sensing Symposium*, volume 2, pages 1401–1403 vol.2, 1999.

[7] D. C. Heinz et al. Fully constrained least squares linear spectral mixture analysis method for material quantification in hyperspectral imagery. *IEEE Transactions on Geoscience and Remote Sensing*, 39(3):529–545, 2001.

[8] L. J. Janik, J. Skjemstad, K. Shepherd, and L. Spouncer. The prediction of soil carbon fractions using mid-infrared-partial least square analysis. *Soil Research*, 45(2):73–81, 2007.

[9] B. Keating and P. Carberry. Emerging opportunities and challenges for australian broadacre agriculture. *Crop and Pasture Science*, 61(4):269–278, 2010.

[10] N. Keshava and J. F. Mustard. Spectral unmixing. *IEEE Signal Processing Magazine*, 19(1):44–57, 2002.

[11] Y. Kuzyakov, I. Subbotina, H. Chen, I. Bogomolova, and X. Xu. Black carbon decomposition and incorporation into soil microbial biomass estimated by 14c labeling. *Soil Biology and Biochemistry*, 41(2):210 – 219, 2009.

[12] D. A. Manning and E. Lopez-Capel. Test procedures for determining the quantity of biochar within soils. *Biochar for Environmental Management–Science and Technology*, pages 301–316, 2009.

[13] J. M. Nascimento and J. M. Dias. Vertex component analysis: A fast algorithm to unmix hyperspectral data. *IEEE Transactions on Geoscience and Remote Sensing*, 43(4):898–910, 2005.

[14] V. P. Pauca, J. Piper, and R. J. Plemmons. Nonnegative matrix factorization for spectral data analysis. *Linear algebra and its applications*, 416(1):29–47, 2006.

[15] Y. Qian, S. Jia, J. Zhou, and A. Robles-Kelly. Hyperspectral unmixing via $L_{1/2}$ sparsity-constrained nonnegative matrix factorization. *IEEE Transactions on Geoscience and Remote Sensing*, 49(11):4282–4297, 2011.

[16] D. Seung and L. Lee. Algorithms for non-negative matrix factorization. *Advances in neural information processing systems*, 13:556–562, 2001.

[17] K. A. Spokas, K. B. Cantrell, J. M. Novak, D. W. Archer, J. A. Ippolito, H. P. Collins, A. A. Boateng, I. M. Lima, M. C. Lamb, A. J. McAloon, et al. Biochar: a synthesis of its agronomic impact beyond carbon sequestration. *Journal of Environmental Quality*, 41(4):973–989, 2012.

[18] J. Wang and C.-I. Chang. Applications of independent component analysis in endmember extraction and abundance quantification for hyperspectral imagery. *IEEE Transactions on Geoscience and Remote Sensing*, 44(9):2601–2616, 2006.

[19] M. E. Winter. N-FINDR: an algorithm for fast autonomous spectral end-member determination in hyperspectral data. In *SPIE International Symposium on Optical Science, Engineering, and Instrumentation*, pages 266–275. International Society for Optics and Photonics, 1999.

[20] D. Woolf, J. E. Amonette, F. A. Street-Perrott, J. Lehmann, and S. Joseph. Sustainable biochar to mitigate global climate change. *Nature communications*, 1:56, 2010.